The Sintering, Sintered Microstructure and Mechanical Properties of Ti-Fe-Si Alloys

Y.F. YANG, S.D. LUO, G.B. SCHAFFER, and M. QIAN

A systematic study has been conducted of the sintering, sintered microstructure and tensile properties of a range of lower cost Ti-Fe-Si alloys, including Ti-3Fe-(0-4)Si, Ti-(3-6)Fe-0.5Si, and Ti-(3-6)Fe-1Si (in wt pct throughout). Small additions of Si (≤1 pct) noticeably improve the as-sintered tensile properties of Ti-3Fe alloy, including the ductility, with fine titanium silicides (Ti_5Si_3) being dispersed in both the α and β phases. Conversely, additions of >1 pct Si produce coarse and/or networked Ti_5Si_3 silicides along the grain boundaries leading to predominantly intergranular fracture and, hence, poor ductility, although the tensile strength continues to increase because of the reinforcement by Ti_5Si_3. Increasing the Fe content in the Ti-*x*Fe-0.5/1.0Si alloys above 3 pct markedly increases the average grain size and changes the morphology of the α-phase phase to much thinner and more acicular laths. Consequently, the ductility drops to <1 pct. Si reacts exothermically with Fe to form Fe-Si compounds prior to the complete diffusion of the Fe into the Ti matrix during heating. The heat thus released in conjunction with the continuous external heat input melts the silicides leading to transient liquid formation, which improves the densification during heating. No Ti-TiFe eutectoid was observed in the as-sintered Ti-Fe-Si alloys. The optimum PM Ti-Fe-Si compositions are determined to be Ti-3Fe-(0.5-1.0)Si.

DOI: 10.1007/s11661-012-1272-8

I. INTRODUCTION

COST reduction has been the main thrust of Ti research and development ever since Ti became an industrially important metal in 1948.[1] The high cost of a Ti component arises from the Ti metal itself as well as the manufacturing process, which in many cases, determines the Ti use level.[2] The conventional cold-compaction-and-sinter powder metallurgy (PM) approach is technically the simplest and economically the most attractive PM near-net shape manufacturing process, which is compatible with nonfatigue critical applications.[2–4] In this context, subsequent cost reduction of PM Ti components will depend largely on the availability of lower cost PM Ti alloys that offer desired properties. This requires the use of affordable Ti powder and inexpensive alloying elements.

The −100 mesh hydrogenated-dehydrogenated (HDH) Ti powder offers a reasonable basis for current PM Ti alloy development because of its affordable price and moderate oxygen content. It is expected to be a prime cost-affordable Ti powder source for the future PM Ti market. As a low-cost β-Ti stabilizer, Fe has been used in a variety of commercial Ti alloys, including Ti-5Al-2.5Fe, Ti-6Al-2Fe, Ti-10V-2Fe-3Al, and Ti-4.5Fe-6.8Mo-1.5Al (in wt pct throughout) and the emerging TIMETAL 54M (Ti-5Al-4V-0.6Mo-0.4Fe) and TIMETAL 18 (Ti-5V-5Mo-5.5Al-2.3Cr-0.8Fe).[5–8] In addition, small additions of Fe improve both the machinability and hot workability of Ti alloys such as KS EL-F (Ti-4.5Al-4Cr-0.5Fe-0.15C) and TIMETAL 54M.[7,8] From a PM standpoint, Fe is a fast diffuser in both α-Ti and β-Ti.[9] For example, Fe was found to be essentially uniform in a blended elemental Ti-10V-2Fe-3Al when heated at 5 K/min to just 1473 K (1200 °C).[10] A faster diffuser may favor the self-diffusion of the base atoms[11] and enhance densification. Compared with other β-Ti stabilizers, Fe markedly reduces the solidus of the Ti-Fe alloys (*e.g.*, the solidus of Ti-5Fe [pct] is 1723 K [1450 °C] *vs* 1873 K [1600 °C] for Ti-5Cr [pct], 1913 K [1640 °C] for Ti-5V [pct], 1958 K [1685 °C] for Ti-5Mo [pct], and 1943 K [1670 °C] for Ti). This makes Ti-Fe based alloys more suited to solid state sintering. However, the most attractive attribute of Fe from a microstructure design perspective is that Ti-TiFe eutectoid does not form in Ti-Fe alloys even subject to very slow cooling rates.[12] This avoids the brittle TiFe phase.

A range of PM Ti-Fe alloys has thus been assessed.[9,12–17] Chen *et al.*[12] sintered Ti-3Fe, Ti-5Fe, and Ti-7Fe (pct) blends made from low oxygen (0.134 pct) fine Ti powder (25 μm) and Fe (3.4 μm) powder. Excellent properties were obtained from each alloy, particularly the as-sintered Ti-7Fe, which attained tensile properties similar to wrought Ti-6Al-4V. However, the resulting mechanical properties of these alloys become much less attractive (the ductility drops from 13 pct to 2 pct for Ti-7Fe) when fabricated with HDH Ti powder containing (0.25 to 0.35) pct O.[13–17]

Y.F. YANG and S.D. LUO, Postdoctoral Research Fellows, G.B. SCHAFFER, Professor, and M. QIAN, Reader in Materials, are with The University of Queensland, School of Mechanical and Mining Engineering, ARC Centre of Excellence for Design in Light Metals, Brisbane, Queensland 4072, Australia. Contact e-mail: ma.qian@uq.edu.au
Manuscript submitted November 21, 2011.

Published online: 06 July 2012

Silicon is another inexpensive alloying element and is much lighter (2.33 g/cm^3) than Ti. Small additions of Si have been used in several commercial Ti alloys by the ingot metallurgy approach to improve their resistance to creep and oxidation.[18–20] In contrast, the use of Si in PM Ti alloys has been limited. Recent work[21] shows that small additions of Si can noticeably enhance the sintering and mechanical properties of the Ti-3Ni (pct) alloy without decreasing the ductility. This article presents a detailed assessment of the potential of the Ti-Fe-Si system as lower cost PM Ti alloys. First, the effect of Si on the microstructure and mechanical properties of Ti-3Fe was investigated systematically. The composition of Ti-3Fe (pct) is selected in the first instance because it gives the best combination of as-sintered strength and ductility when fabricated with –100 mesh HDH Ti powder.[15,17] Based on the optimum Si content determined, the effect of Fe content was subsequently investigated.

II. EXPERIMENTAL PROCEDURE

Sumitomo HDH Ti powder (–100 mesh, ≤150 μm, 99.5 pct purity, 0.25 pct O; Sumitomo Corporation, Kyoto, Japan), elemental Fe powder (≤45 μm, 99.5 pct purity), and Si powder (≤45 μm, 99.5 pct purity) supplied by the CERAC Inc. (Farmington, NH) were used. Powder mixtures of Ti-3Fe-xSi (x = 0 to 4, in pct) and Ti-xFe-0.5/1Si (x = 3 to 6) were prepared in a Turbula mixer for 30 minutes. The elemental blends were compacted uniaxially in a floating die into samples of 10 mm in both diameter and height for sintering experiments, and into tensile bars of 56 mm × 11 mm × 4.5 mm for mechanical testing, both at 400 MPa. Acrawax C (Lonza Inc., Allendale, NJ) was applied lightly to the die wall to reduce wear and friction.

The powder compacts were sintered at 1573 K (1300 °C) for 120 minutes in a vacuum of 10^{-3} to 10^{-2} Pa with heating and cooling rates of 4 K/min. Differential scanning calorimetry (DSC) (Model STA 409CD; Netzsch, Wittelsbacherstraße, Germany) was used to analyze the thermal events during heating and cooling where samples were heated to 1573 K (1300 °C) and then cooled to 473 K (200 °C) in high-purity argon, both at 10 K/min. In addition, DSC experiments were interrupted at characteristic temperatures by flowing argon at a cooling rate of 40 K/min. X-ray diffraction (XRD, D8 Advance, Cu K_α target, Bruker AXS, Madison, WI) was used to determine the phase evolution process. The sintering response was examined using a high-sensitivity (1.25 nm/digit) dilatometer (Model Netzsch 402C, Netzsch, Wittelsbachestraße, Germany) in high purity-argon with both heating and cooling at 10 K/min.

Sintered samples were sectioned longitudinally, polished using 50 nm colloidal alumina, and etched with Kroll's etchant. They were examined by scanning electron microscopy (SEM) (Model JEOL 6460L; JEOL Ltd., Tokyo, Japan) equipped with energy-dispersive spectrometer (EDS) (JEOL Ltd.). Software Image-Pro plus 5.0 (Media Cybernetics, Bethesda, MD) was used to quantify the grain size of the as-sintered microstructures. Tensile specimens (3 mm × 4.5 mm cross-section and 15 mm gauge length) were machined from as-sintered bars and tested on an Instron screw machine (Model 5054, Instron Corporation, Norwood, MA) with a crosshead speed of 0.5 mm/min. A contact extensometer was used to measure tensile strain. Three samples were tested for each condition. The oxygen and nitrogen contents were analyzed by a LECO nitrogen/oxygen analyzer (Model TC-136; LECO Corporation, St. Joseph, MI). Thermo-Calc Software AB (Thermo-Calc Software 2008, Stockholm, Sweden) and Ti-alloys database V3 (TTTI3) were used for thermodynamic assessment.

III. RESULTS

A. *Thermodynamic Predictions*

Figure 1 shows the effect of Si on the equilibrium solid and liquid fractions in the Ti-3Fe-xSi alloys predicted by Thermo-Calc. The solidus of Ti-3Fe-xSi decreases with increasing Si content. The minimum Si content for persistent liquid formation in the Ti-3Fe alloy at 1573 K (1300 °C) (the selected sintering temperature) is 2.4 pct. Further increasing the Si content will lower the solidus to <1573 K (1300 °C). The maximum solubility of Si in α-Ti is <0.3 pct. These predictions suggest that Si has the potential to enhance the sintering of Ti-3Fe and to strengthen the alloy by precipitation of Ti_5Si_3 silicides.

B. *Sintered Density and Sintering Response*

Figure 2 shows the relative green and sintered densities of Ti-3Fe-(0-4)Si alloys after sintering at 1573 K (1300 °C) for 120 minutes as a function of the Si content. The poor compressibility of the Si powder led to a slight decrease in the green density. The sintered density increases with increasing Si content up to 3 pct.

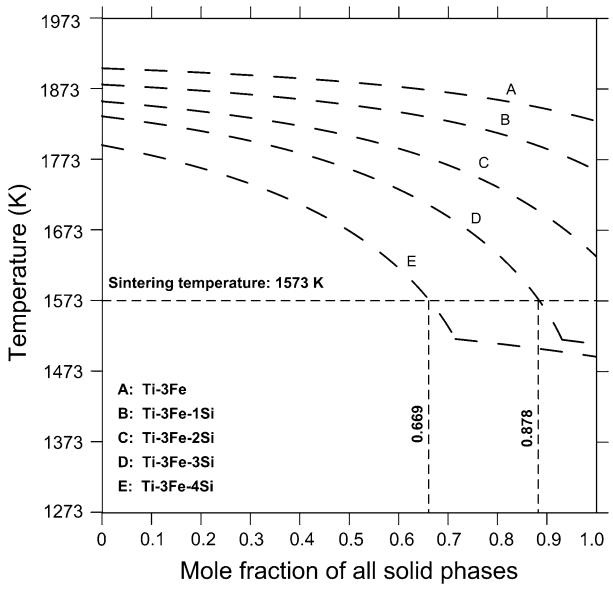

Fig. 1—Thermo-Calc predictions of the equilibrium solid and liquid fractions of Ti-3Fe-xSi alloys using Ti-alloys database V3 (TTTI3).

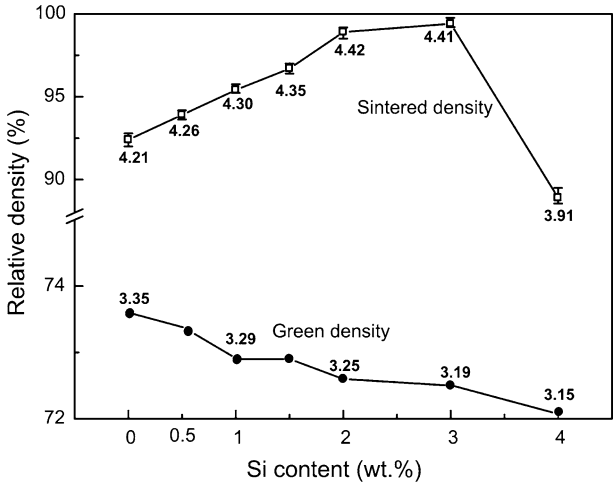

Fig. 2—Green and sintered densities of Ti-3Fe-*x*Si alloys as a function of the Si content. Sintering was conducted at 1573 K (1300 °C) for 120 min in vacuum. The actual density is shown at each data point (g/cm^3).

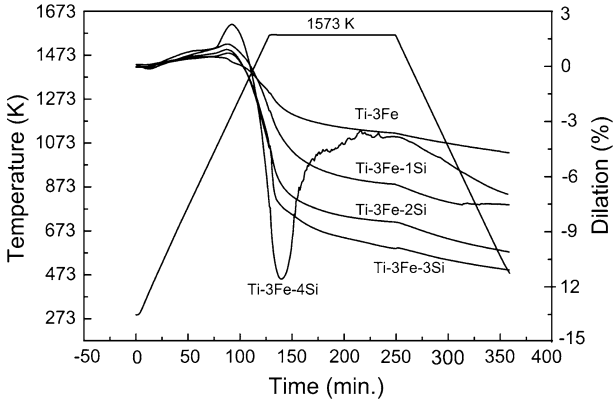

Fig. 3—Dilation curves of Ti-3Fe, Ti-3Fe-1Si, Ti-3Fe-2Si, Ti-3Fe-3Si, and Ti-3Fe-4Si during heating to 1573 K (1300 °C) at 10 K/min, 120 min hold at 1573 K (1300 °C), and subsequent cooling to 473 K (200 °C) at 10 K/min.

Near full densification is obtained at 2 pct Si even though no persistent liquid is predicted. A substantial decrease in the sintered density occurred at 4 pct Si, accompanied by sample slumping because of excessive liquid formation,[22,23] where the Ti-3Fe-4Si alloy is predicted to contain ~0.331 mole fraction of liquid at 1573 K (1300 °C) (Figure 1). These results indicate that Si is effective in enhancing the sintering of Ti-3Fe, but its addition should be limited to ≤3 pct.

The dilatometry of the Ti-3Fe-*x*Si ($x = 0, 1, 2, 3, 4$) alloys is shown in Figure 3. It supports the introduction of ≤3 pct Si for consistent shrinkage. The Ti-3Fe-4Si alloy showed two expansion events, one at ~1173 K (900 °C) during heating probably a result of transient liquid formation and the other at temperatures close to the isothermal hold temperature.

C. *Phase Formation and Evolution During Heating*

Figure 3 shows that noticeable shrinkage occurred during heating. To understand the phase formation and

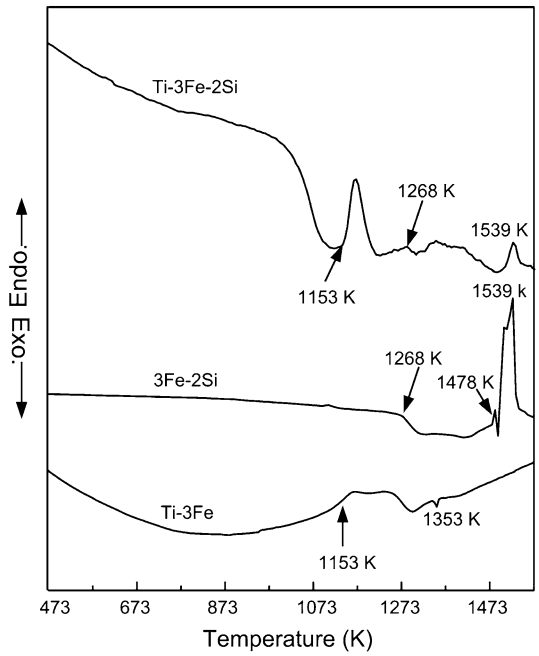

Fig. 4—DSC curves of loose powder blends of Ti-3Fe, 3Fe-2Si, and Ti-3Fe-2Si during heating to 1573 K (1300 °C) at 10 K/min in high purity argon.

evolution during heating, DSC experiments were interrupted and cooled to room temperature at 40 K/min by flowing cooling water. Because of the weak DSC signals obtained from the Ti-3Fe-1Si alloy, a Ti-3Fe-2Si alloy was studied instead. In addition, both Ti-3Fe and 60Fe-40Si (pct) (equivalent to 3Fe-2Si) were studied by DSC for additional details. The results are summarized in Figure 4. Figure 5 shows the XRD spectra for each DSC sample. The following observations are notable:

- Ti-3Fe: An endothermic peak occurred at ~1153 K (~880 °C), corresponding to the α-Ti → β-Ti transformation, whereas the exothermic peak at 1353 K (1080 °C) corresponds to the formation of the TiFe intermetallics detected by XRD (Figure 5).
- 3Fe-2Si: An exothermic peak is observed from ~1268 K (~995 °C) as a result of the slow solid-state diffusion reaction, corresponding to the formation of Fe_3Si and $FeSi_2$ indentified by XRD from the DSC sample interrupted at 1268 K (995 °C). Two endothermic peaks are observed at 1478 K (1205 °C) and 1539 K (1266 °C), implying liquid formation.
- Ti-3Fe-2Si: The endothermic peak at ~1153 K (~880 °C) should correspond to the α-β transformation, similar to that detected for the Ti-3Fe. In addition, an exothermic peak developed from ~1268 K (~995 °C) while an endothermic peak occurred at ~1539 K (1266 °C), which is similar to those observed for the binary 3Fe-2Si alloy. No exothermic peak appeared at 1353 K (1080 °C). XRD of the DSC sample interrupted at 1268 K (995 °C) revealed the presence of both Fe_3Si and $FeSi_2$. This is also similar to those observed in the binary 3Fe-2Si. The major

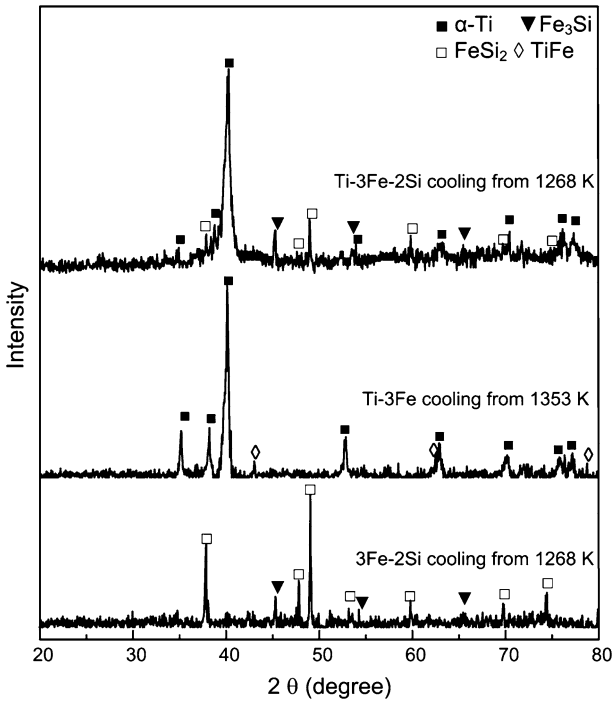

Fig. 5—XRD patterns of Ti-3Fe, 3Fe-2Si, and Ti-3Fe-2Si samples from interrupted DSC experiments. Cooling rate to room temperature was 40 K/min.

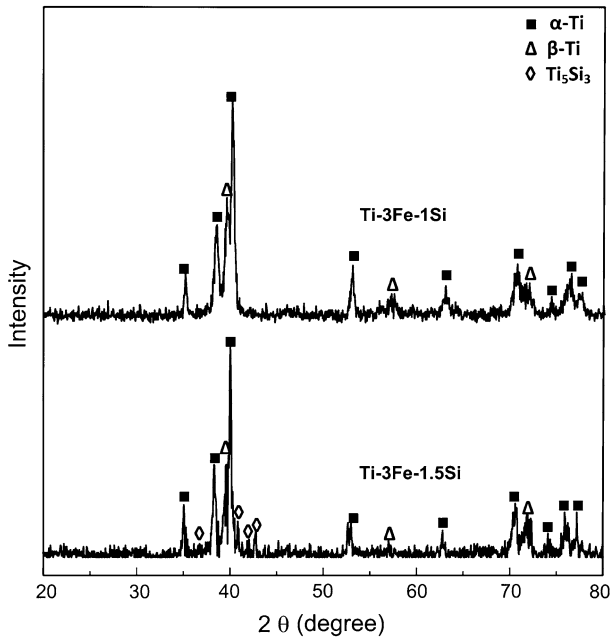

Fig. 6—XRD patterns of Ti-3Fe-1Si and Ti-3Fe-1.5Si sintered at 1573 K (1300 °C) for 120 min in vacuum.

reactions in the powder compacts of Ti-3Fe-2Si during heating to 1573 K (1300 °C) are, thus, those between Fe and Si.

D. *Microstructure*

Figure 6 shows the effect of increasing the Si content on the phase constituents of the as-sintered Ti-3Fe alloy. Apart from the α-Ti phase, β-Ti is detected in the as-sintered Ti-3Fe-*x*Si ($x = 1, 1.5$) alloys. However, no titanium silicides were detected until the Si content reached 1.5 pct. Figure 7 shows the as-sintered microstructures of the Ti-3Fe-*x*Si alloys ($x = 0, 0.5, 1.0, 1.5$, and 2.0). The long, dark gray laths are α-Ti, whereas the intragranular light gray laths are β-Ti. Together they form α-β colonies in the as-sintered microstrucutre.

Although absent from the XRD spectra, fine precipitates are observed in both the α and β phases in the as-sintered Ti-3Fe-*x*Si alloys containing 0.5 pct Si and 1 pct Si (Figure 7(b) and (c)). X-ray mapping revealed that they contain essentially Ti and Si (see the mapping results of Si for the precipitates in Figure 7(c)). TEM analysis was focused on the precipitates in the α phase (Figure 8). The selected-area electron diffraction (SAED) pattern confirmed that they have the Ti_5Si_3 type of crystal structure, hexagonal $D8_8$. TEM energy-dispersive X-ray analysis showed the presence of essentially Ti and Si, Ti63.2Si36.6Fe0.3 (in at. pct) (Figure 8(d)), very close to Ti_5Si_3. In addition, Thermo-Calc calculations indicate that Ti_5Si_3 will precipitate in both the α and β in Ti-3Fe-0.5/1Si alloys (Figure 9). The fine precipitates are thus Ti_5Si_3. These fine silicides exhibit short fiber morphologies formed by precipitation from the β phase during cooling. In contrast, coarse Ti_5Si_3 particles (dark gray) are conspicuous in the as-sintered Ti-3Fe-1.5Si (Figure 7). The presence of Ti_5Si_3 increased with increasing Si content. In addition, their distribution changed from isolated particles to interconnected networks along the grain boundaries (Figure 7(f)).

E. *Mechanical Properties*

1. *The effect of the Si content*

Figure 10 shows the tensile properties of the as-sintered Ti-3Fe-(0-3)Si alloys. Compared with the Ti-3Fe, small additions of Si (≤1 pct) result in a noticeable increase in the tensile properties including the elongation. This can be attributed to the improved sintered density, the dispersion strengthening of the fine silicides in the α and β-Ti matrix, and solid solution strengthening. Additional noticeable increases in the tensile strength are observed with ≥1.5 pct Si because of the formation of more reinforcing Ti_5Si_3 silicides and the increased sintered density. However, this was accompanied by a drop in the ductility (Figure 10(b)) because of the formation of the networked Ti_5Si_3 along the grain boundaries.

Figure 11 shows the fractographs of the as-sintered tensile samples of Ti-3Fe-*x*Si ($x = 0, 1, 1.5$, and 2). When the Si content is ≤1.0 pct, cleavage facets and residual pores are typical features of the fracture surfaces. Few fractured Ti_5Si_3 particles were observed. In contrast, fractured Ti_5Si_3 particles were readily visible on the fracture surfaces of the 1.5 pct Si alloy (Figure 11(d)). In addition, increasing the Si content to 2 pct resulted in predominantly intergranular fracture (Figure 11(e)), corresponding to the networked brittle Ti_5Si_3 phase along the grain boundaries (Figure 7(f)). Fractured Ti_5Si_3 silicides were observed on the fractured

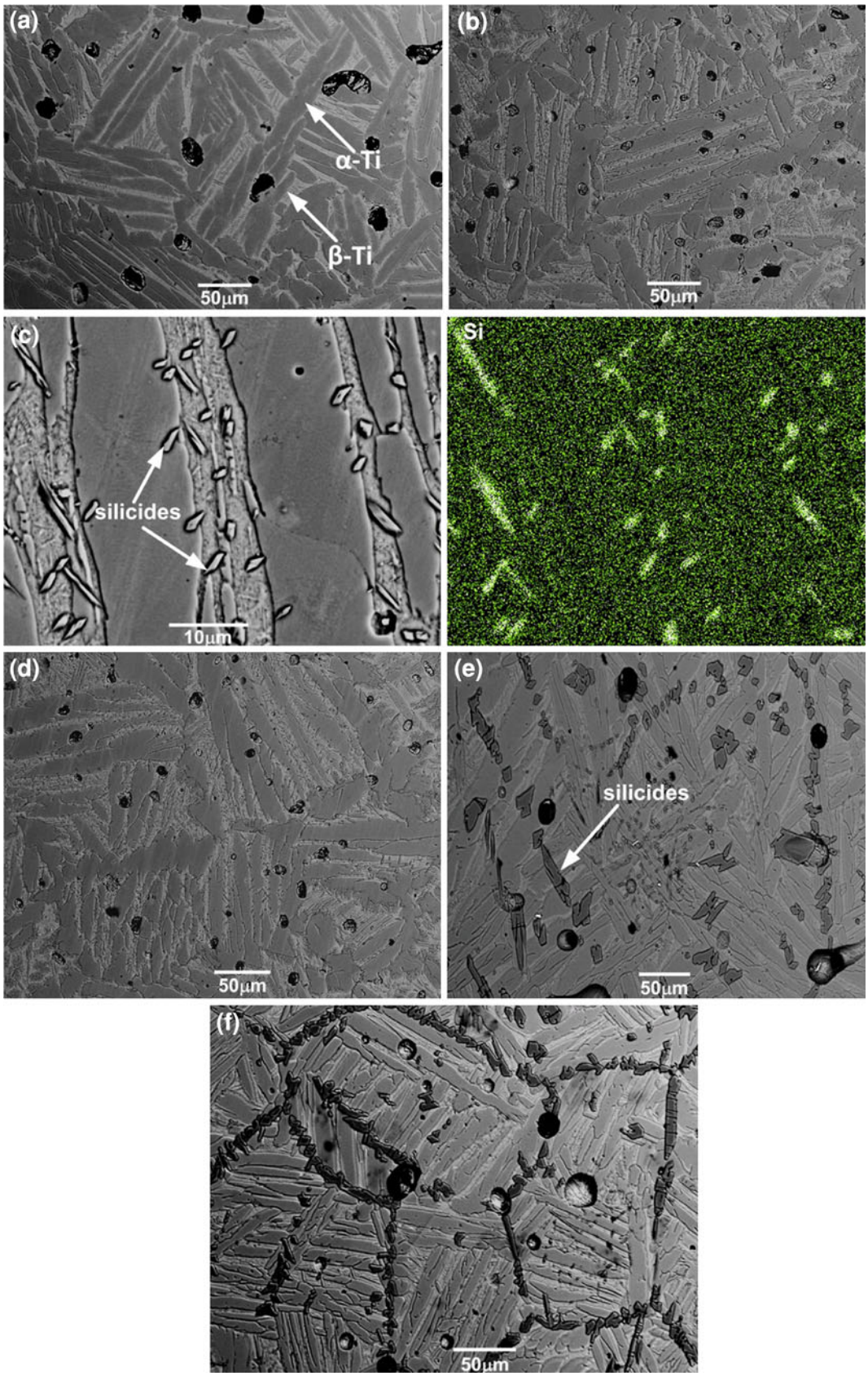

Fig. 7—SEM backscattered electron (BSE) images of the as-sintered microstructures of Ti-3Fe-*x*Si (in pct) after 120 min at 1573 K (1300 °C) in vacuum: (*a*) 0 pct Si, (*b*) 0.5 pct Si, (*c*) an enlarged view showing fine precipitates in the β phase and the associated X-ray mapping results of Si for the precipitates, (*d*) 1 pct Si, (*e*) 1.5 pct Si, and (*f*) 2 pct Si, showing networked titanium silicides.

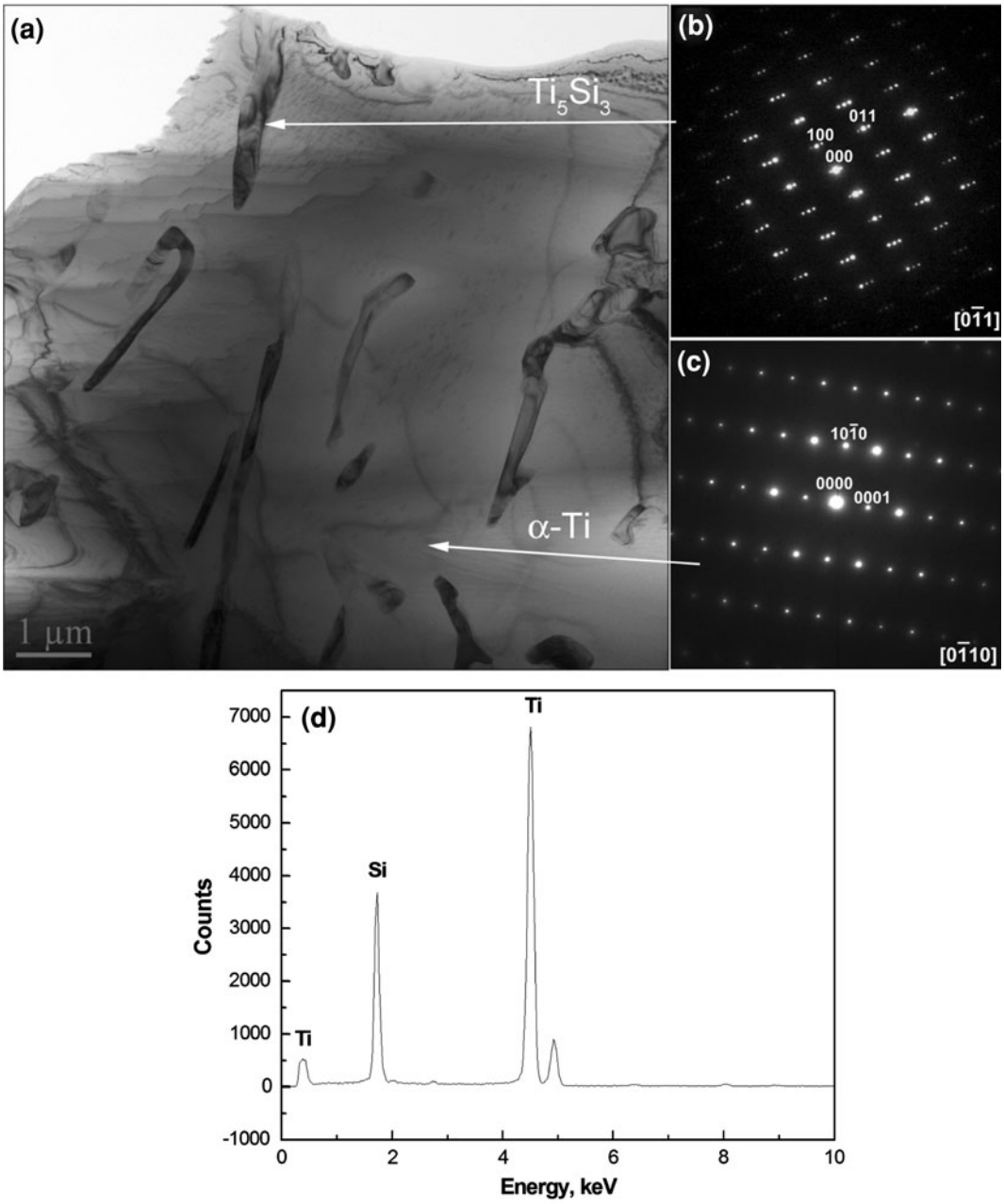

Fig. 8—TEM analysis of the fine precipitates in the α phase: (*a*) a bright-field image, (*b*) and (*c*) SAED patterns taken from the marked areas in (*a*), and (*d*) TEM energy-dispersive X-ray results of precipitates.

surfaces of Ti-3Fe-1.5Si, whereas the as-sintered Ti-3Fe-2Si showed predominantly intergranular fracture.

2. *The effect of the Fe content*

Based on the influence of the Si content, Ti-*x*Fe-0.5Si and Ti-*x*Fe-1Si alloys containing 4, 5, and 6 pct Fe were sintered and assessed. Figure 12 shows the sintered densities and tensile properties of the Ti-*x*Fe-0.5Si and Ti-*x*Fe-1Si alloys. Increasing the Fe content increased both the sintered density and tensile strength (Figure 12(a)), but the ductility dropped sharply (see Figure 12(b)).

Figure 13 shows the average grain size of the as-sintered Ti-*x*Fe-0.5Si and Ti-*x*Fe-1.0Si ($x = 3, 4, 5,$ and 6) alloys as a function of the Fe content. A significant increase in the grain size is observed with increasing Fe content. In addition to grain coarsening, another noticeable change arising from the increased Fe content is the change in the morphology of the α-Ti phase. Figure 14 shows the as-sintered microstructures of Ti-*x*Fe-0.5Si ($x = 3, 4,$ and 6). The α-Ti phase becomes much thinner and more acicular in most grains.

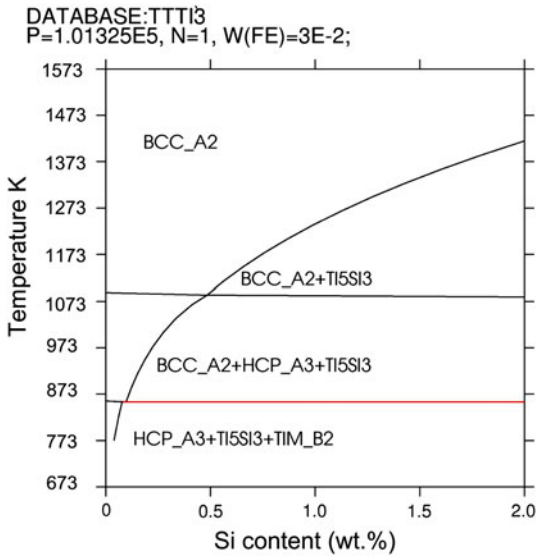

Fig. 9—Thermo-Calc predictions of the phase diagram of Ti-3Fe-*x*Si alloys up to 2 pct where Ti-3Fe is defined as the base alloy. TIM_B2 refers to TiFe, BCC_A2 is β-Ti and HCP-A3 is α-Ti.

IV. DISCUSSION

A. *Mechanism of Enhanced Sintering by Si*

The sintering of Ti-3Fe during heating to, and at isothermal hold of, 1573 K (1300 °C), is solid-state sintering (achieved only 92.4 pct theoretical density [TD] after 1573 K [1300 °C] for 120 minutes). With an addition of 3 pct Si, the amount of persistent liquid is predicted to be ~0.122 mole fraction at 1573 K (1300 °C) (Figure 1). The Ti-3Fe-3Si alloy was thus sintered to near full density. However, with no persistent liquid being predicted at 1573 K (1300 °C), the Ti-3Fe-2Si alloy was similarly sintered to a high density (99.0 pct TD). This deals with the reactions between Si and Fe.

Figures 4 and 5 revealed that Fe and Si reacted to form low-melting point Fe_3Si and Fe_2Si at ~1268 K (~995 °C) during heating. This temperature is lower than the temperature at which Fe completely diffuses into the Ti particles. At a heating rate of 5 K/min, Fe particles of 97 μm in the powder compacts of Ti-7Fe exist up to 1363 K (1090 °C),[16] whereas Fe particles of 19 μm do not disappear until 1298 K (1025 °C) in the powder compacts of Ti-5Fe.[9] The reactions between Fe and Si are exothermic. The heat released in conjunction with the continuous external heat input melts the Fe_3Si and Fe_2Si silicides leading to binary Fe-Si liquid formation at both ~1478 K (~1205 °C) and ~1539 K (1266 °C) (see the DSC curve for Ti-3Fe-2Si in Figure 4). This contributes to sintering densification. It should be pointed out that the formation of these binary liquids and the time for which they exist may depend on the heating rate and the particle (Fe and Si) sizes.[24,25]

Increasing the Si content to 4 pct caused noticeable expansion. A similar expansion event was observed during the sintering of Ti-3Ni-3Si.[21] In both cases, the expansion occurred almost as soon as the isothermal hold started, corresponding to the formation of a massive amount of liquid in a short period of time. It has been proposed that the high liquid volume caused rapid pore closure, and the evolving gas such as chloride vapours from the residual chlorides in the Ti powder was then trapped and caused an increase in pressure inside closed pores.[26]

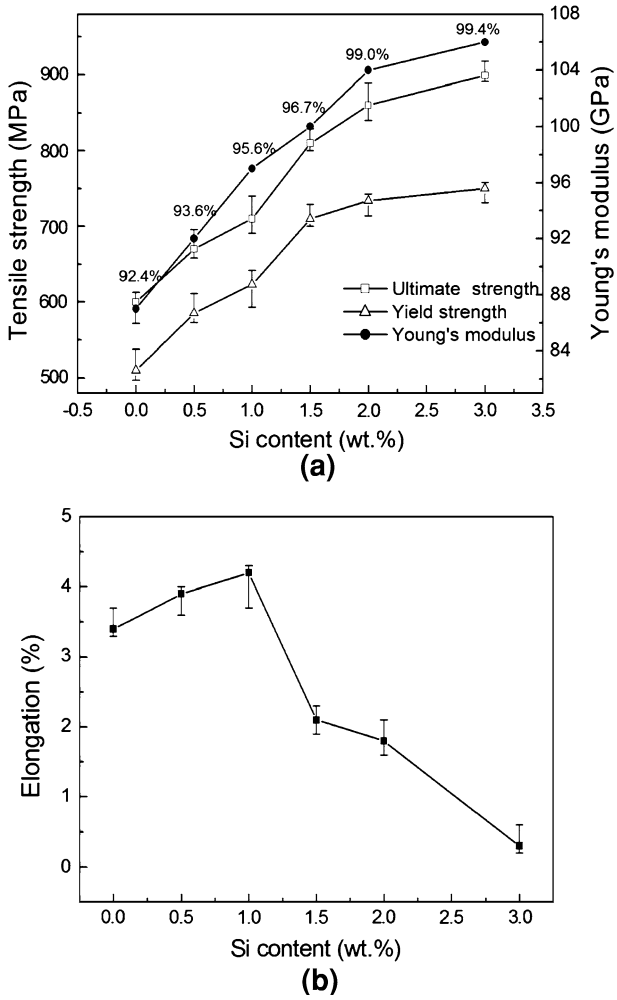

Fig. 10—(*a*) Tensile strength and Young's modulus and (*b*) tensile elongation of Ti-3Fe-*x*Si alloys sintered at 1573 K (1300 °C) for 120 min in vacuum. The figures indicated in (a) are relative sintered densities.

B. *The Effect of Si on the Microstructure and Mechanical Properties*

The tensile ductility of Ti materials is sensitive to their oxygen and nitrogen contents. To clarify this, the oxygen and nitrogen contents in the as-sintered Ti-3Fe-*x*Si (x = 0, 1, and 2, in pct) alloys were analyzed and the results are listed in Table I. The oxygen and nitrogen contents changed slightly with increasing Si content. Hence, the drop in the tensile ductility with increasing Si content above 1 pct is not caused by oxygen and

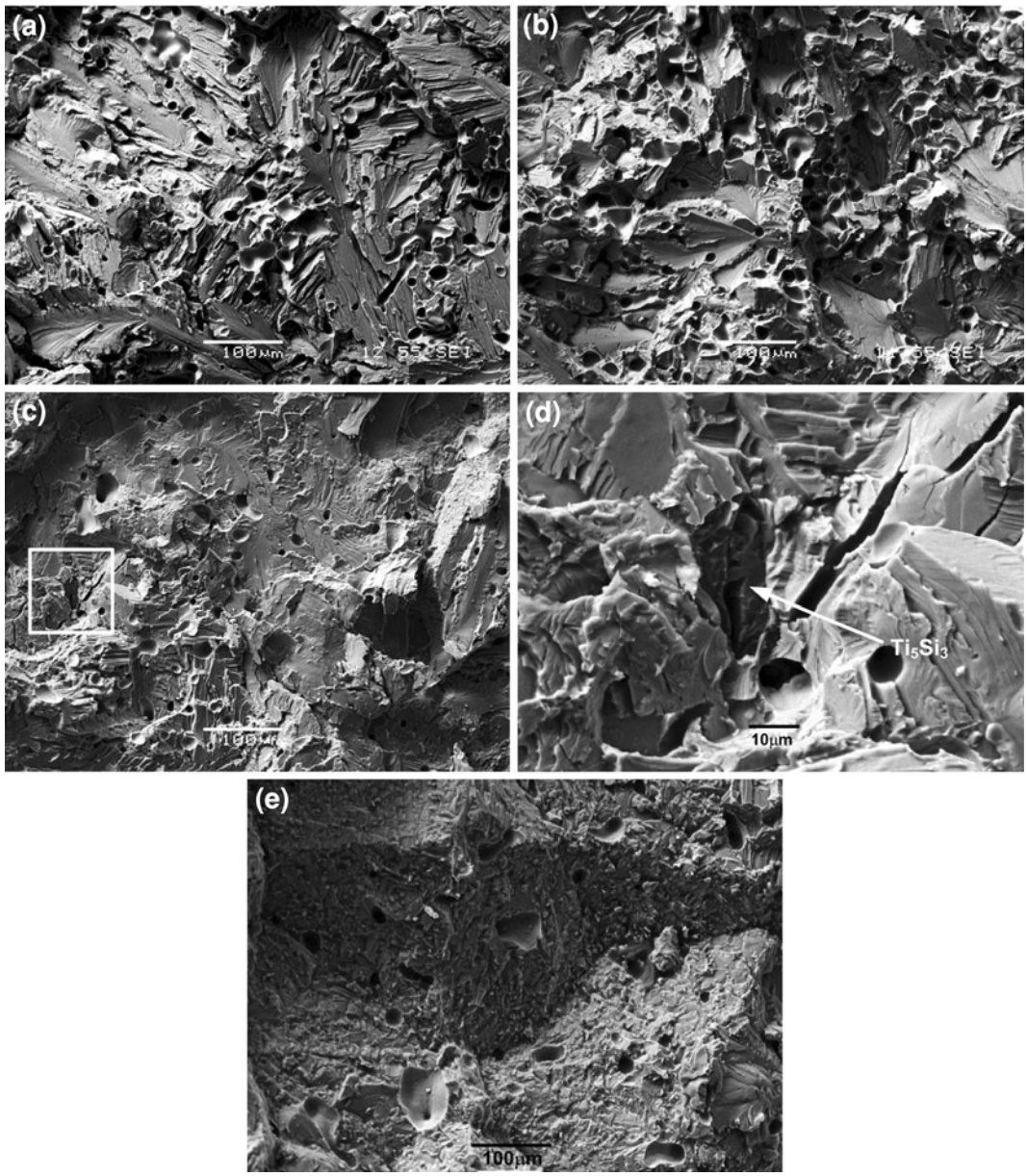

Fig. 11—SEM fractographs of tensile samples from as-sintered Ti-3Fe-*x*Si alloys: (*a*) 0 pct Si, (*b*) 1 pct Si, (*c*) 1.5 pct Si, (*d*) an enlarged view of the area marked in (c) showing a fractured silicide, and (*e*) 2.0 pct Si, showing predominantly intergranular fracture. Sintering was conducted at 1573 K (1300 °C) for 120 min in vacuum.

nitrogen. It is attributed to the formation of the coarse and/or networked Ti_5Si_3 along the grain boundaries. As shown in Figure 11, the fracture mode of the as-sintered Ti-3Fe-*x*Si ($x = 0$, 1, 1.5, and 2) alloys shows clear dependence on the Si content. The fractured Ti_5Si_3 particles that are observed at 1.5 pct Si (Figure 11(d)) and the predominantly intergranular fracture that occurred at 2.0 pct Si (Figure 11(e)) because of the grain boundary Ti_5Si_3 networks (Figure 7(f)) confirms that the Si content should be limited to ≤1.0 pct. Because silicon improves the resistance of titanium alloys to creep and oxidation, these low-cost Ti alloys may have the potential for low-to-medium temperature applications.

C. *The Effect of Fe*

A detailed examination of the as-sintered microstructures of Ti-4Fe-0.5Si and Ti-6Fe-0.5Si found no evidence for the Ti-TiFe eutectoid structure, which is predicted by the phase diagram. Instead, the microstructure consists predominantly of α-Ti and *β*-Ti phases. Similar observations were reported by Chen *et al.*[12] based on TEM characterization of as-sintered Ti-(3-7)Fe alloys. The linear drop in ductility with increasing Fe from 3 pct to 6 pct was, thus, not caused by the formation of the brittle eutectoid TiFe intermetallics.

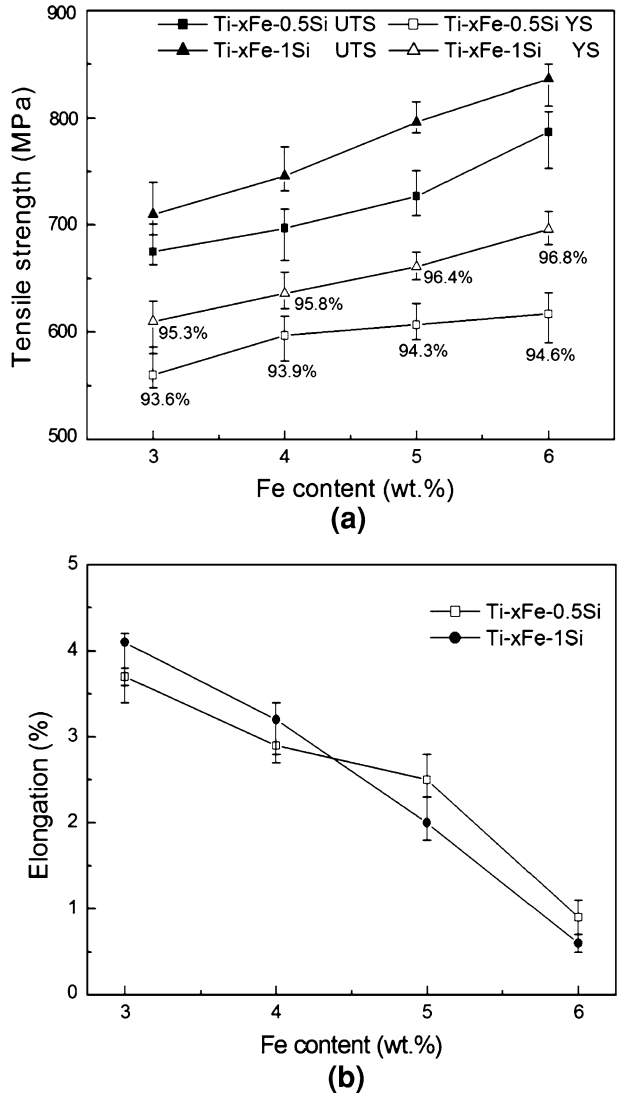

Fig. 12—(*a*) Ultimate tensile strength and yield strength (YS), the figures shown on the curve are relative sintered density. (*b*) Tensile elongation of Ti-*x*Fe-0.5Si and Ti-*x*Fe-1Si alloys with the Fe content being varied from 3 pct to 6 pct, sintered at 1573 K (1300 °C) for 120 min in vacuum.

Increasing the Fe content has in fact introduced two noticeable changes to the as-sintered microstructure. One is that the average grain size increased almost linearly with increasing Fe content (Figure 13). This observation can be attributed to two reasons. The largely reduced solidus of the alloy with increasing Fe content (the decrease is >80 K from Ti-3Fe-0.5Si to Ti-6Fe-0.5Si) favors grain growth with respect to the same sintering temperature. In addition, Fe is a fast diffuser in Ti; it may have enhanced the self-diffusion of Ti for grain growth. The other is that the morphology of the α-Ti phase changes to much thinner and more acicular laths (Figure 14), which is associated with the increased grain size. The morphology of the α-Ti phase is known to affect the ductility, where acicular morphologies are usually detrimental.[10] The change in the morphology of the α-Ti phase arising from the increased Fe content has

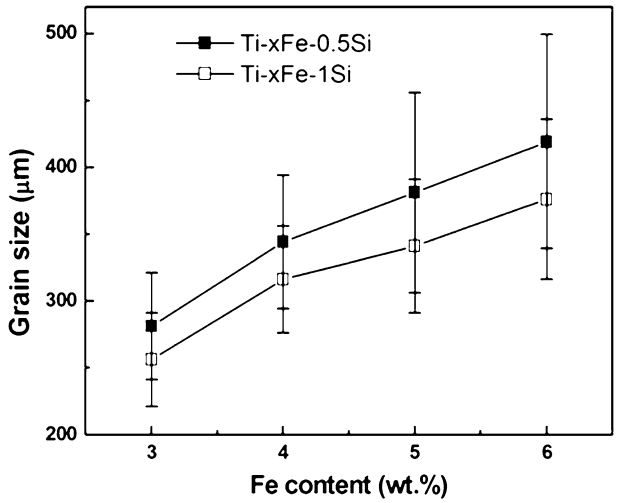

Fig. 13—Average grain size of as-sintered Ti-xFe-0.5Si and Ti-xFe-1.0Si (x = 3, 4, 5, 6, in pct) alloys as a function of the Fe content. Each set of grain size data was averaged from the measurements of 300 grains. Sintering was conducted at 1573 K (1300 °C) in vacuum for 120 min.

an adverse effect on the ductility. These observations indicate that the Fe content should be limited to ~3 pct.

V. SUMMARY

- A small addition of Si (≤1 pct) to Ti-3Fe noticeably improves the tensile properties of the as-sintered alloy including the elongation, due largely to the enhanced densification and formation of fine Ti_5Si_3 dispersoids in both the α and β phases. However, an addition of >1 pct Si leads to the formation of coarse and/or networked Ti_5Si_3 particles along the grain boundaries resulting in predominantly intergranular fracture and poor ductility.
- Increasing the Fe content in the Ti-*x*Fe-0.5/1.0Si alloys beyond 3 pct increases the sintered density and tensile strength but sharply decreases the ductility. The poor ductility results from the coarser grain structures and the change in the morphology of the α-Ti phase to much thinner and more acicular laths. The average grain size increased almost linearly with increasing Fe content in the range from 3 pct to 6 pct.
- Si reacts exothermically with Fe to form Fe-Si compounds prior to the complete diffusion of Fe into the Ti matrix. The heat thus released in conjunction with the continuous external heating melts the Fe-Si silicides leading to the formation of transient liquids, which contribute to the sintering densification observed during heating.

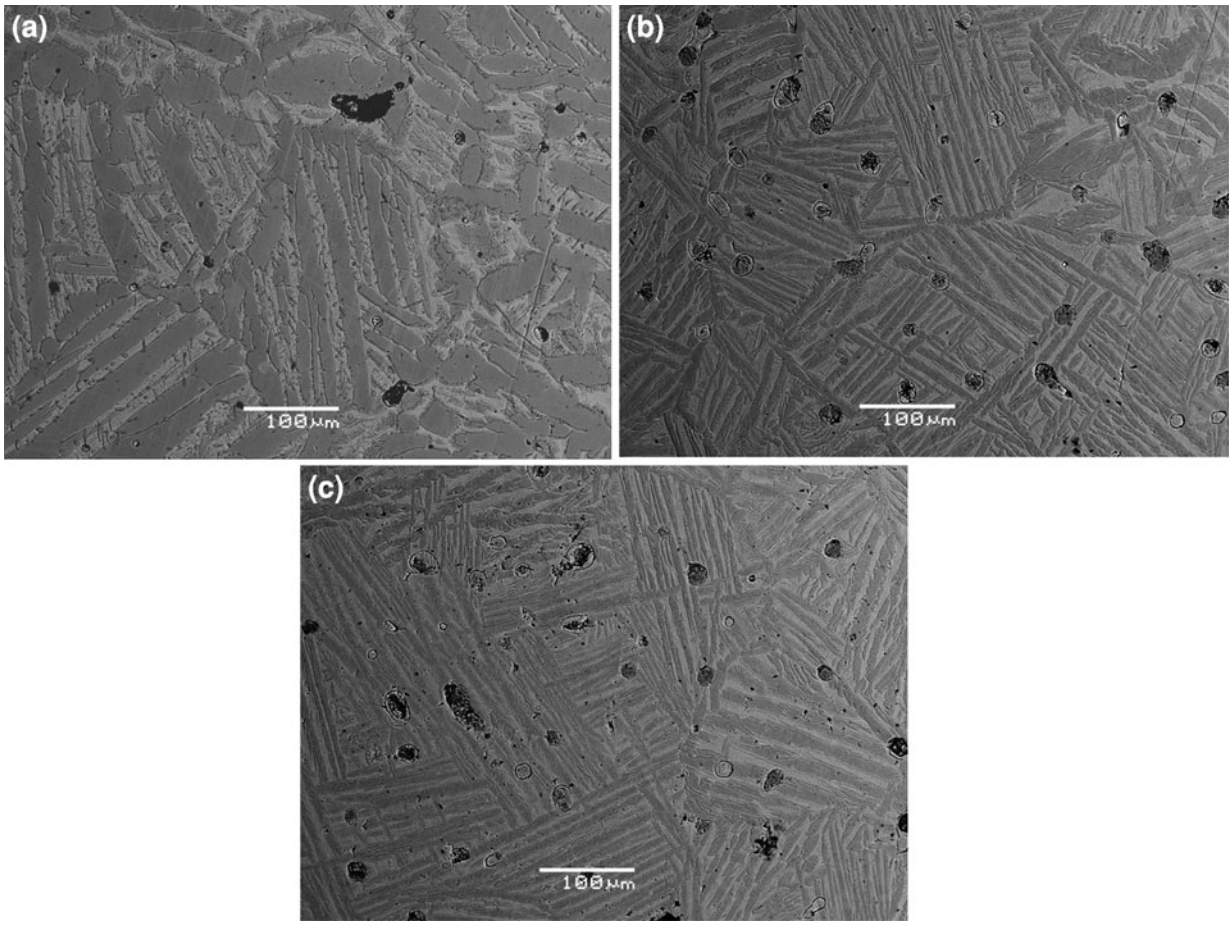

Fig. 14—SEM BSE images showing the change in the morphology of the α-Ti phase laths with increasing Fe content in the as-sintered microstructures of (*a*) Ti-3Fe-0.5Si, (*b*) Ti-4Fe-0.5Si, and (*c*) Ti-6Fe-0.5Si. Sintering was conducted at 1573 K (1300 °C) for 120 min in vacuum.

Table I. Oxygen and Nitrogen Contents in the Tensile Samples Sintered at 1573 K (1300 °C) for 120 min

Alloy Composition (pct)	O (pct)	N (pct)
Ti-3Fe	0.33	0.03
Ti-3Fe-1Si	0.33	0.03
Ti-3Fe-2Si	0.32	0.03

- The optimum PM Ti-Fe-Si compositions are determined to be Ti-3Fe-(0.5-1.0)Si for fabrication with the –100 mesh HDH Ti powder.

ACKNOWLEDGMENTS

This work was funded by the Australian Research Council (ARC) through the Center of Excellence for Design in Light Metals and an Australian Postdoctoral Fellowship for Y.F. Yang. Dr. Ming Yan of The University of Queensland performed the TEM work for this paper (Figure 8).

REFERENCES

1. D.C. Li, H. Liu, and D.L. Zhou: *Titanium Smelting Technologies*, Chemical Industry Press, Beijing, China, 2009, pp. 209–14.
2. M. Qian: *Int. J. Powder Metall.*, 2010, vol. 46 (5), pp. 29–44.
3. H. Nakajima, K. Yusa, and Y. Kondo: *Scripta Mater.*, 1996, vol. 34, pp. 249–53.
4. Z.Z. Fang: *Int. J. Powder Metall.*, 2010, vol. 46, pp. 9–17.
5. D.B. Lee, K.B. Park. H.W. Jeong, and S.E. Kim: *Mater. Sci. Eng. A.*, 2002, vol. 328 pp. 161–68.
6. TIMETAL Datasheets, TIMETAL 10-2-3, http://www.timet.com.
7. S. Murakami, K. Ozaki, K. Ono, and Y. Itsumi: *R&D Kobe Steel Engineering Reports*, 2010, vol. 60 pp. 37–41.
8. TIMETAL Datasheets, TIMETAL 54M, http://www.timet.com.
9. W. Wei, Y. Liu, K. Zhou, and B. Huang: *Powder Metall.*, 2003, vol. 46, pp. 246–50.
10. Y.F. Yang, S.D. Luo, G.B. Schaffer, and M. Qian: *Mater. Sci. Eng. A.*, 2011, vol. 528, pp. 6719–26.
11. J.F. Murdocki and C.J. Mcharguet: *Acta Metall.*, 1968, vol. 16, pp. 493–500.
12. B.Y. Chen, K.S. Hwang, and K.L. Ng: *Mater. Sci. Eng. A.*, 2011, vol. 528, pp. 4556–63.
13. H. Kyogoku, S. Komatsu, K. Shinohara, H. Jinushi, and T. Toda: *J. Jpn. Soc. Powder Metall.*, 1994, vol. 41, pp. 1075–79.
14. H. Kyogoku, S. Komatsu, I. Tsuchitori, and T. Toda: *J. Jpn. Soc. Powder Metall.*, 1995, vol. 42, pp. 1052–56.
15. P.G. Esteban, E.M. Ruiz-Navas, and E. Gordo: *Mater. Sci. Eng. A.*, 2010, vol. 527, pp. 5664–69.
16. P.G. Esteban, L. Bolzoni, E.M. Ruiz-Navas, and E. Gordo: *Powder Metall.*, 2011, vol. 54, pp. 242–52.
17. Y. Liu, L.F. Chen, H.P. Tang, C.T. Liu, B. Liu, and B.Y. Huang: *Mater. Sci. Eng. A.*, 2006, vol. 418, pp. 25–35.

18. M.R. Winstone, R.D. Rawlings, and D.R.F. West: *J. Less-Common Metals*, 1975, vol. 39, pp. 205–17.
19. P.J. Bania, A.J. Hutt, R.E. Adams, and W.M. Parris: *Titanium '92' Science and Technology*, F.H. Froes and I. Caplan, eds., TMS, Warrendale, PA, 1993, p. 2787.
20. P.G. Allen, P.J. Bania, A.J. Hutt, and Y. Combres: *Titanium '95' Science and Technology*, P.A. Blenkinsop, W.J. Evans, and H.M. Flower, eds., IOM, Cambridge, U.K., 1995, p. 1938.
21. Y.F. Yang, S.D. Luo, G.B. Schaffer, and M. Qian: *Mater. Sci. Eng. A.*, 2011, vol. 528, pp. 7381–87.
22. R.M. German: *Liquid Phase Sintering*, Plenum Press, New York, NY, 1985, p. 162.
23. P. Boch and J. C. Niepce: *Ceramic Materials: Processes, Properties and Applications*, ISTE, London, U.K., 2007, p. 59.
24. R.N. Lumley and G.B. Schaffer: *Scripta Mater.*, 1996, vol. 35, pp. 589–95.
25. R.N. Lumley and G.B. Schaffer: *Scripta Mater.*, 1998, vol. 39, pp. 1089–94.
26. I.M. Robertson and G.B. Schaffer: *Powder Metall.*, 2010, vol. 53, pp. 27–33.